Title
PHOTOPROTONS PRODUCED BY 245+15 Mev GAMMA RAYS ON CARBON

Author
Cence, Robert J.

Publication Date
1959-11-01

UCRL 8921

UNIVERSITY OF CALIFORNIA

Ernest O. Lawrence

Radiation Laboratory

PHOTOPROTONS PRODUCED BY 245±15–Mev GAMMA RAYS ON CARBON

UCRL-8921
Physics and Mathematics
TID-4500 (15th Ed.)

UNIVERSITY OF CALIFORNIA
Lawrence Radiation Laboratory
Berkeley, California

Contract No. W-7405-eng-48

PHOTOPROTONS PRODUCED BY 245±15-Mev GAMMA RAYS ON CARBON

Robert J. Cence

(Thesis)

November 1959

Printed for the U. S. Atomic Energy Commission

Printed in USA. Price $1.50. Available from the
Office of Technical Services
U. S. Department of Commerce
Washington 25, D.C.

PHOTOPROTONS PRODUCED BY 245±15-Mev GAMMA RAYS ON CARBON

Contents

PHOTOPROTONS PRODUCED BY 245±15-Mev GAMMA RAYS ON CARBON

Robert J. Cence

Lawrence Radiation Laboratory
University of California
Berkeley, California

November 1959

ABSTRACT

An experiment was performed, using the method of Weil and McDaniel, in which the interactions arising from 245±15 Mev were selected out of all those produced by the bremsstrahlung spectrum of gamma rays from the Berkeley 342-Mev synchrotron. These interactions were selected by requiring a coincidence between each interaction and the degraded electron that produced the selected gamma ray.

The energy spectrum of protons produced at 60 deg (lab) by these selected gamma rays impinging on a carbon target was measured. This spectrum covered a range from 105 Mev to 250 Mev. A rather precise analysis was made by using the quasi-deuteron model of Levinger. In contrast with previous analyses, conservation of both momentum and energy were taken into account in a fairly accurate way. The results of the analysis depend on the momentum distribution of the centers of mass assumed for the quasi deuterons. The momentum distribution that gave the best fit to the data is given by the sum of two Gaussian functions, one with a 1/e value of 1.6 Mev and the other with a 1/e value of 30 Mev. This result is given considerable discussion.

I. INTRODUCTION

Many experimenters have measured the energy distribution of photoprotons produced by high-energy gamma rays on light nuclei.[1, 2, 3, 4] The most dominant feature of this distribution is the large number of high-energy protons produced at large angles. This was interpreted by Levinger to mean that the incoming photons interact with a small subunit in the nucleus--in particular, a neutron-proton pair which he called a quasi deuteron.[5] The mechanism of this interaction, although similar to that of photodisintegration of the deuteron, is modified by the momentum distribution of the quasi deuterons in the nucleus. Levinger showed that it was necessary for this process that the neutron-proton pair be very close together. Under this condition the wave function of the quasi deuteron is just a multiple of that of the free deuteron. The quasi deuterons are then in the S states. This interaction is thus proportional to the photodisintegration cross section of the free deuteron, suitably averaged over the momentum distribution of the quasi deuterons. It was assumed that the 25% quasi deuterons in the singlet S state do not have a photodisintegration cross section so dramatically different from those in the triplet S state that the results of the theory would have been significantly altered.

The basic validity of this model has been verified by observing conjugate neutrons and protons in coincidence.[6, 7, 8, 9] It is now possible by using this model, to calculate the momentum spectrum of neutron-proton pairs in the nucleus from the energy spectrum of ejected photoprotons.

It must be pointed out that detailed experimental comparison with the theory is not easily obtained. This is because high-energy photon beams are produced by bremsstrahlung of electrons so that the gamma rays have a continuous spectrum of energies with approximately a $1/E$ dependence up to the energy of the initial electrons. This has the effect of smoothing out the proton spectrum and thus masking the details of the interaction.

In order to gain more detailed information Weil and McDaniel in 1953 attempted to select out gamma rays in a small energy interval (by a method which we used in this experiment also).[4]

They used this technique to observe the spectrum of protons from carbon due to 190-Mev gamma rays. However, the energy resolution obtained was rather broad (± 30 Mev), and furthermore, the electronic apparatus was very complicated because they were trying to attain time resolutions not then easily obtainable. They concluded that it would probably have been just as easy to perform the experiment by successively reducing the energy of the accelerator and using the subtraction technique.

Since the experiment of Weil and McDaniel, counting techniques have developed to such an extent that coincidence resolving times of a few millimicroseconds with high efficiency and electronic stability are readily available. For this reason we thought it was worth while to attempt another experiment with selected gamma rays, and further to try to attain improved resolution.

II. EXPERIMENTAL METHOD

A. General

The 340-Mev Berkeley synchrotron was used for this experiment. The electron beam was accelerated to full energy and then the accelerating voltage was allowed to taper off while the magnetic field was still rising. This caused the electrons to spiral in until they struck a tantalum converter located at a reduced radius. These electrons then produced a bremsstrahlung spectrum of gamma rays. The residual electrons, now with greatly reduced energy, were deflected toward the center of the accelerator and momentum-analyzed by its guide field. Since the characteristic angle for bremsstrahlung is $M_e c^2/E \sim 0.1^\circ$ at 340 Mev, where E is the energy of the initial electrons, the residual electrons were deflected toward the center of the accelerator in a narrow band in the plane of the electron orbits. Thus it was possible to place a scintillator in such a position that it was traversed by all the residual electrons in a selected energy interval only. Since the converter was a material with large atomic weight it did not absorb by recoil any appreciable energy in the bremsstrahlung process. (However, the converter had to be very thin in order that scattering of the residual electrons be kept small. In this case it was 0.0013 in. thick.). Hence, the energy of the gamma rays associated with the electrons traversing the scintillator was given simply by $E-E'$, where E' is the energy of the residual electrons traversing the scintillator. The experiment was performed in the gamma-ray beam, and by demanding a coincidence, with appropriate delay, between the experimental events and the electron counter those events due to the gamma rays of energy $E-E'$ were selected out.

In this experiment the energy spectrum of protons from carbon was observed at $60^\circ \pm 8^\circ$. The target was a $4 \times 4 \times 1/2$-inch slab of carbon placed so that the plane of the slab was perpendicular to the direction of the proton telescope. This meant that the beam traversed the target at an angle of 30° with respect to the plane of the target. A plan view of the experimental set-up is shown in Fig. 1.

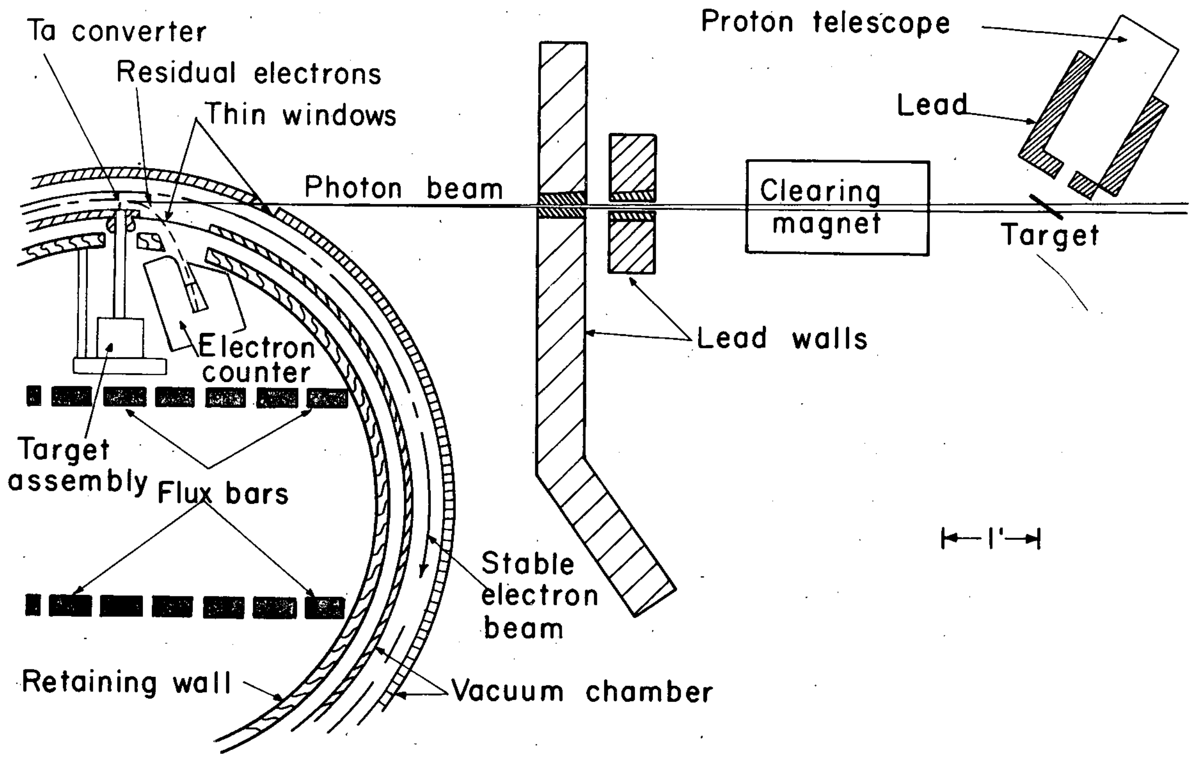

MU-18805

Fig. 1. Plan view of the experimental setup.

B. Electron Counter

1. Description of Counter

The electron counter as it finally evolved consisted of a plastic scintillator 1-3/8×1-3/8×4 inches with a 1P21 photomultiplier tube located about 2 inches above it and viewing the scintillator by means of a lucite light pipe as shown in Fig. 2. The 1P21 was surrounded by a triple iron shield which was in turn surrounded by a lead radiation shield. The iron shield weighed about 40 lb and was water-cooled in order to reduce heating due to the alternating guide field of the accelerator. The radiation shield was not made of pure lead, again because of the heating problem, but rather was formed by pressing lead powder in a base of plastic cement. It had about 70% the density of pure lead and was 8 inches thick. The whole assembly was mounted on a wooden platform which was wedged between the magnet yokes with jack screws. The scintillator was located about 10 inches from the center of the accelerator vacuum chamber. The lead shield had a 1×1×4-inch hole in front of the scintillator for collimation, with a 1-inch carbon cube inserted in the hole to eliminate low-energy background.

The magnetic field at the counter reached a maximum of 2600 gauss. Even with the water cooling of the iron shield and the high-resistivity lead-plastic radiation shield, the temperature inside the counter was typically 95°F. It was continuously monitored by a thermocouple.

One octant of the accelerator vacuum chamber had a slot cut through the inside wall over which was cemented 0.005 in. of aluminum. The placement was such that the residual electrons traversed only the thin window upon leaving the chamber. This made scattering negligible.

To obtain pulses of sufficient height it was necessary to operate the 1P21 photomultiplier tube at 2100 volts. At this voltage and with the high counting rates encountered in this experiment, the average current drawn by the 1P21 became quite large during the 3 to 4 milliseconds that the electrons were striking the internal target of the

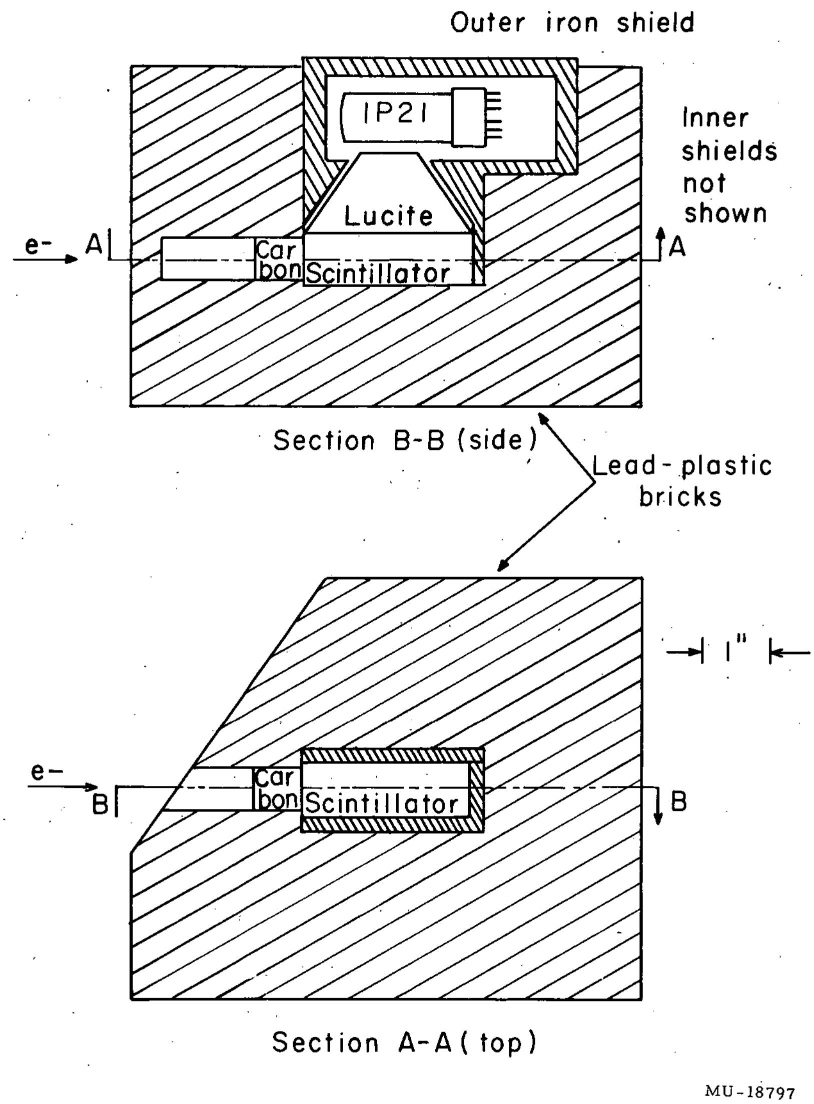

Fig. 2. Horizontal and vertical sections through the electron counter.

synchrotron. To stabilize the dynodes against fluctuations in voltage due to these currents, a voltage divider drawing 0.01 amp current was placed across them. This made a significant contribution to the heating of the counter. Furthermore, a 10-μf capacitor was placed between the last dynode and the common ground.

2. Calibration

The electron counter was calibrated by means of a single-channel pair spectrometer. To determine the efficiency of the electron counter it was merely necessary to compare the number of gamma rays recorded by the pair spectrometer alone at each energy with the number of gamma rays recorded when a coincidence was demanded between the pair spectrometer and the electron counter. This calibration was thus independent of the efficiency of the pair spectrometer. Furthermore, the energy resolution of the spectrometer (3.7%) was small enough in comparison with the resolution of the electron counter that it was not necessary to fold it out of the spectrum obtained.

The spectrum of gamma rays selected by the electron counter is shown in Fig. 3. The peak of the spectrum occurred at 245 Mev, with a full width at half maximum of 30 Mev. There were two contributions to the width. The first was the finite width of the scintillator. This contributed about 10 Mev. The remaining 20 Mev was a result of the fact that the electron beam was spilled into the converter over a period of 3 to 4 milliseconds. Because the guide field was sinusoidal the initial electrons had an energy spread which contributed to the selected gamma-ray spectrum. This long spill-out time was necessary to reduce accidental events.

A somewhat disturbing feature of the electron counter was that it had only 10% efficiency for counting electrons. Tests with a radioactive source when the synchrotron magnetic field was off indicated that 1800 volts should have been sufficient to give adequate pulse height. The fact that 2100 volts was necessary under experimental conditions indicated that the magnetic shield was not quite adequate. However, because the counter was already an imposing structure and because we thought that more iron might perturb the synchrotron magnetic field so

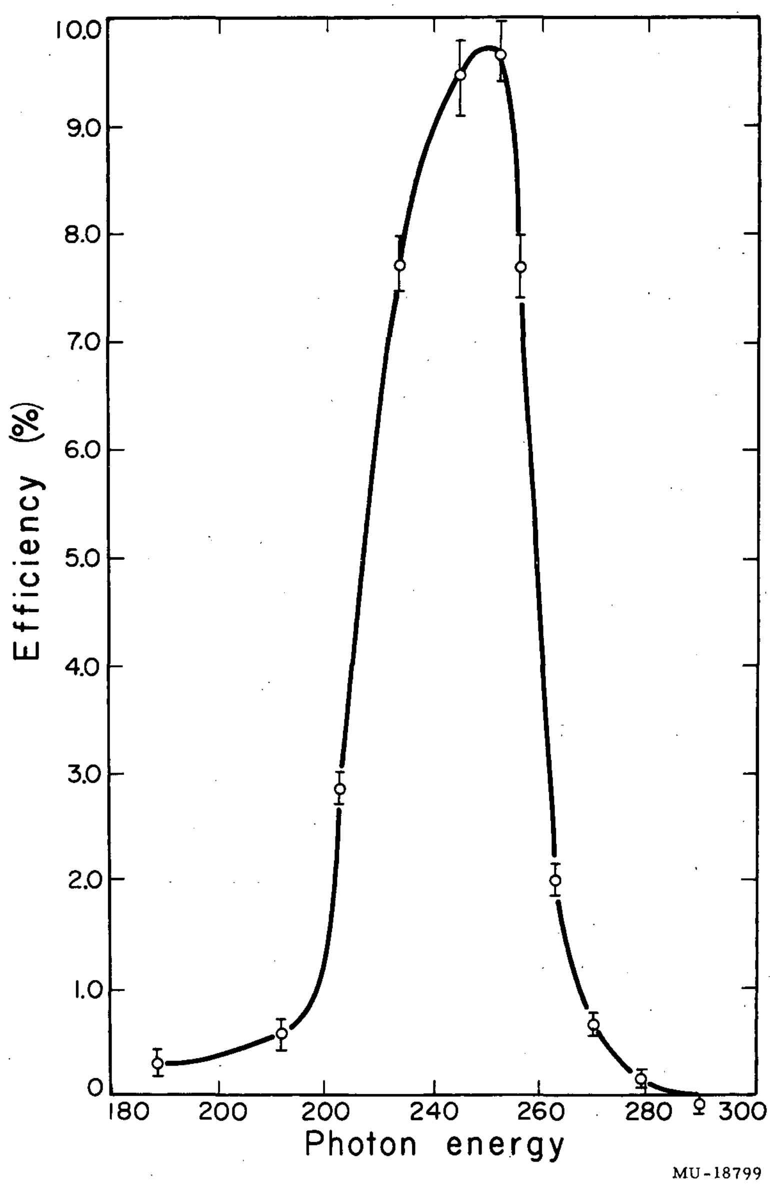

Fig. 3. Plot of the efficiency of the electron counter for counting electrons versus the energy of the associated gamma ray. The curve is drawn for illustrative purposes only. It represents the selected photon spectrum.

that it would be difficult to obtain a beam of electrons, we decided to perform the experiment with the counter as it existed rather than enlarge it.

The residual electrons whose orbits allowed them to enter the electron counter had an energy 90±5 Mev. Since this energy was so well defined, any fluctuation in the electron counter efficiency could not change the spectrum of selected photons. Also, since the whole energy spectrum of protons was observed simultaneously by a multichannel proton telescope, changes in the efficiency of the electron counter could not affect the shape of this spectrum. It could have introduced an error in the absolute magnitude of the results without, however, changing the spectral shape. The efficiency was observed, nevertheless, to be quite constant.

C. Proton Telescope

The proton telescope was designed and constructed by Dwight Dixon.[10] It consisted of

(a) a small scintillator to define the solid angle;

(b) a large scintillator to measure dE/dx; and

(c) a series of ten scintillators, hereafter called range counters, separated by copper absorbers. All the scintillators were viewed by 1P21 photomultiplier tubes except the dE/dx scintillator, which was viewed by a 6655 photomultiplier. A schematic drawing of the telescope is shown in Fig. 4.

A coincidence between the dE/dx counter and the defining counter was used to trigger a 517 Textronix oscilloscope. The signals from the range counters and the dE/dx counter were tapped onto a coaxial delay line (as shown in Fig. 5) so that they could be consecutively displayed on the oscilloscope. The traces were then photographed on 35-mm film.

To reach the first range counter it was necessary for a proton to have 90 Mev energy, and to reach the last range counter, 250 Mev energy. This energy range was divided up into nine intervals by

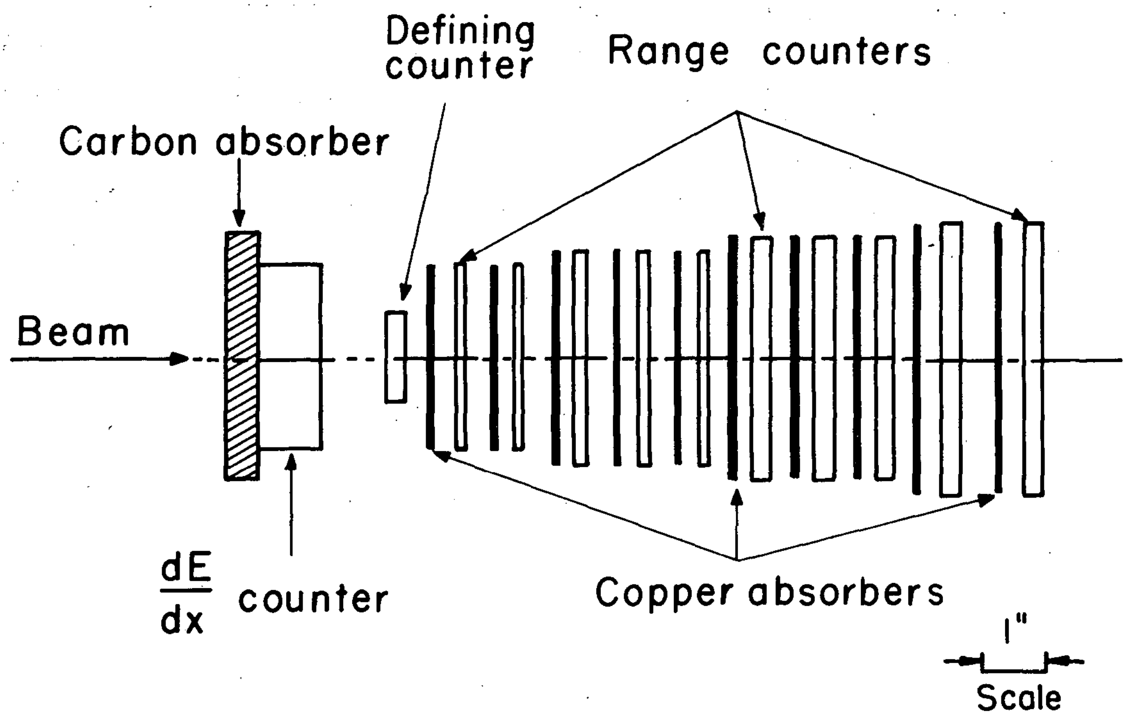

MU-18806

Fig. 4. Proton telescope geometry. All counters are plastic scintillator.

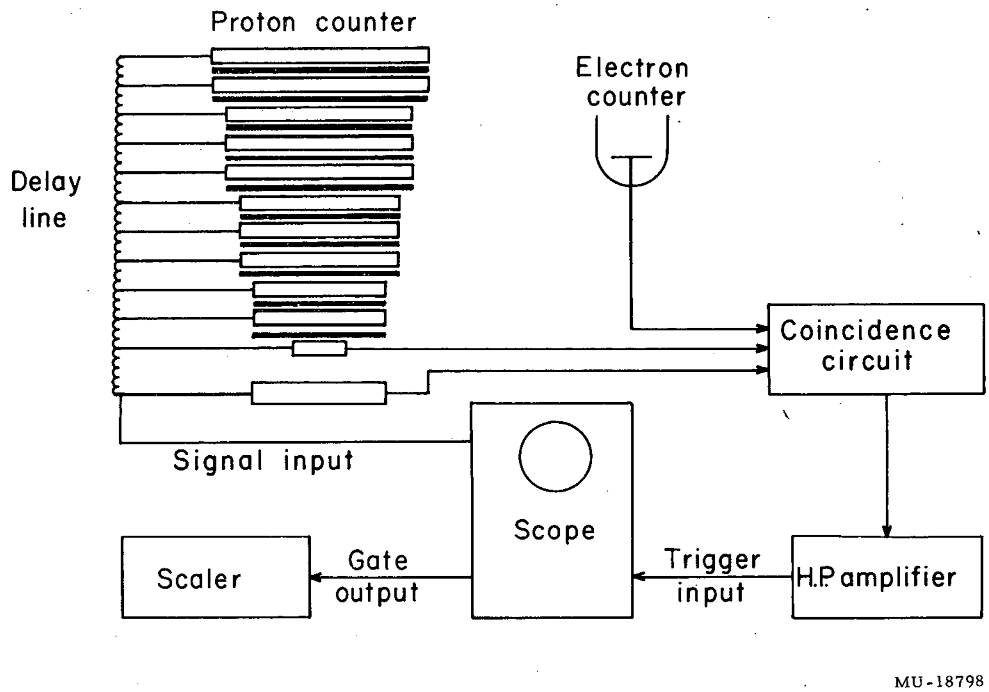

Fig. 5. Block diagram of the electronics.

the ten range counters in the telescope. The first four intervals were 15 Mev each, and the last five were 20 Mev each. An event was said to be associated with range interval No. 1 if a pulse was recorded in range counter No. 1, but not in range counter No. 2; with range interval No. 2 if pulses were recorded in range counters Nos. 1 and 2 but not in No. 3; with range interval No. 3 if pulses were recorded in range counters Nos. 1, 2, and 3 but not in No. 4; etc.

The efficiency of the various range counters was checked by observing how often a range pulse was missing from a series of range pulses. It was found that the efficiency of all the range counters was essentially 100%.

The required corrections to the proton telescope data, to account for scattering and straggling of the particles, are discussed below in Section IV. C.

D. Electronics

A block diagram of the electronics is shown in Fig. 5. The threefold coincidence circuit had a resolving time of about 3 millimicroseconds.[11] This short resolving time was necessary because the electron counter registered counts at a peak rate of 10^5 per second. The proton telescope registered particles at the rate of a few per second. Coincidences between the electron counter and the proton telescope occurred at the rate of a few per hour.

III. COLLECTION OF DATA

To keep accidental counts reasonably low it was necessary to operate the synchrotron about 1% of full beam intensity. This corresponded to 2×10^{7} equivalent quanta per minute. Events were recorded at the rate of 6 per hour. Of these, analysis showed that 3 per hour were protons and the remainder, mesons and electrons. Of the protons, 1 per hour was an accidental. Thus, protons from selected quanta were recorded at the rate of 2 per hour. A total of 694 protons was observed, of which 248 were accidentals. The total number of protons from selected quanta was thus 446.

To determine the number of accidentals, runs were taken with the electron counter pulses delayed by a time large compared with the resolving time of the coincidence circuit. This delay was made equal to one revolution time of the electrons in the accelerator in order to eliminate a possible systematic error due to the bunching of these electrons. The appropriate delay was 2.1×10^{-8} sec, which was about 7 times the resolving time of the coincidence circuit. Runs with and without the added delay were alternated every 2 hours throughout the experiment. This was necessary because of the widely fluctuating beam intensity characteristic of this type of accelerator. The number of alternations was about 50. The accidental runs were normalized to the real runs by means of a thick-walled ionization chamber of the Cornell type placed in the gamma-ray beam.

Because the spectrum of accidentals was the same as that obtained from the full bremsstrahlung beam, runs were taken without the electron counter. The sum of all the protons recorded with bremsstrahlung was then normalized to the sum of all protons from the accidental runs to give a more accurate determination of the accidental spectrum, especially at the higher energies, where the counting rate was low.

IV. TREATMENT OF DATA

A. Reading and Plotting of the Data

The photographed traces were projected by means of a Recordak reader. Each trace contained from 1 to 11 pulses. The height of the first pulse, which was from the dE/dx counter, was measured by means of a template, and the number of pulses after the first was recorded. The height of the first pulse was proportional to the differential ionization of the particle entering the telescope. The number of pulses after the first gave the range of the particle. No traces were read which did not have at least one range pulse in addition to the dE/dx pulse. Sample traces are shown in Fig. 6.

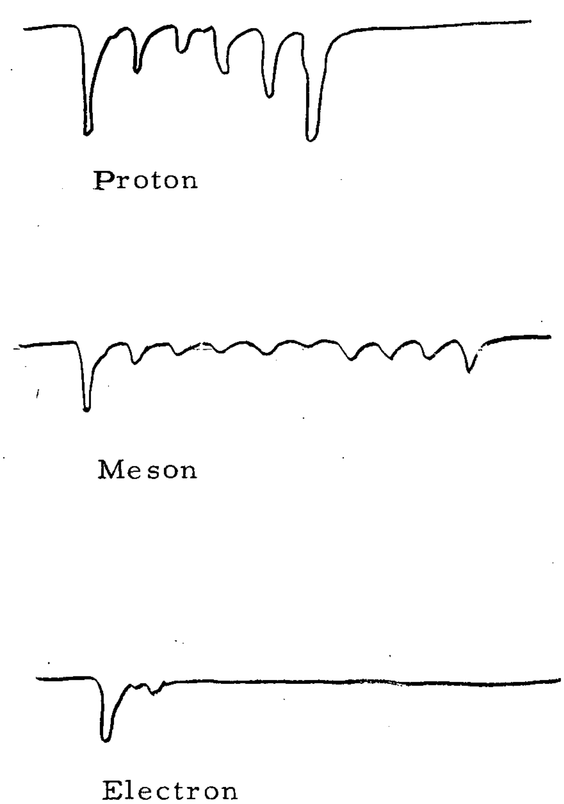

Fig. 6. Sample Oscilloscope traces.

The data are shown plotted in Fig. 7. Each histogram represents the spectrum of pulse heights from the dE/dx counter in those events whose range interval is indicated along the abscissa. Thus, each histogram represents the pulse-height spectrum in a single range interval. Some of the events in Fig. 7 are due to accidental coincidences between the electron counter and the proton telescope. These were determined separately as previously mentioned. The pulse-height spectra due to these accidental coincidences were similar to those in Fig. 7 and were readily subtracted. The number of accidental coincidences was about 50% of the number of true coincidences.

B. Identification of Protons

From Fig. 6 it will be observed that on each of the histograms in the range intervals corresponding to the lower energies there are two pronounced peaks. For example, the histogram in range interval No. 2 has a peak at a pulse height of 22 and another one at a pulse height of 14. The upper peak in each range interval corresponds to the proton events and the lower one to the meson events. This was deduced in two ways. First, in each range interval the ratio of the relative pulse heights at the two peaks was measured and found to be just that expected from protons and mesons. Second, the relative pulse height expected from both protons and mesons as a function of range was calculated, and indeed the position of the upper peaks shows the range-interval dependence expected of protons and the lower peaks the range-interval dependence expected of mesons.

At the lower energies it is clear that one gets a good mass separation between mesons and protons. But at the higher energies the separation is not as evident. The protons should still be separated from the mesons, but the number of events is so small that the spectrum has not been able to developed sufficiently to make the separation clear. At the higher energies, therefore, the protons could not be identified from the histogram alone. For these cases the appropriate proton pulse-height spectrum was determined from a calibration run at the Berkeley 184-inch cyclotron wherein the proton telescope was placed in a

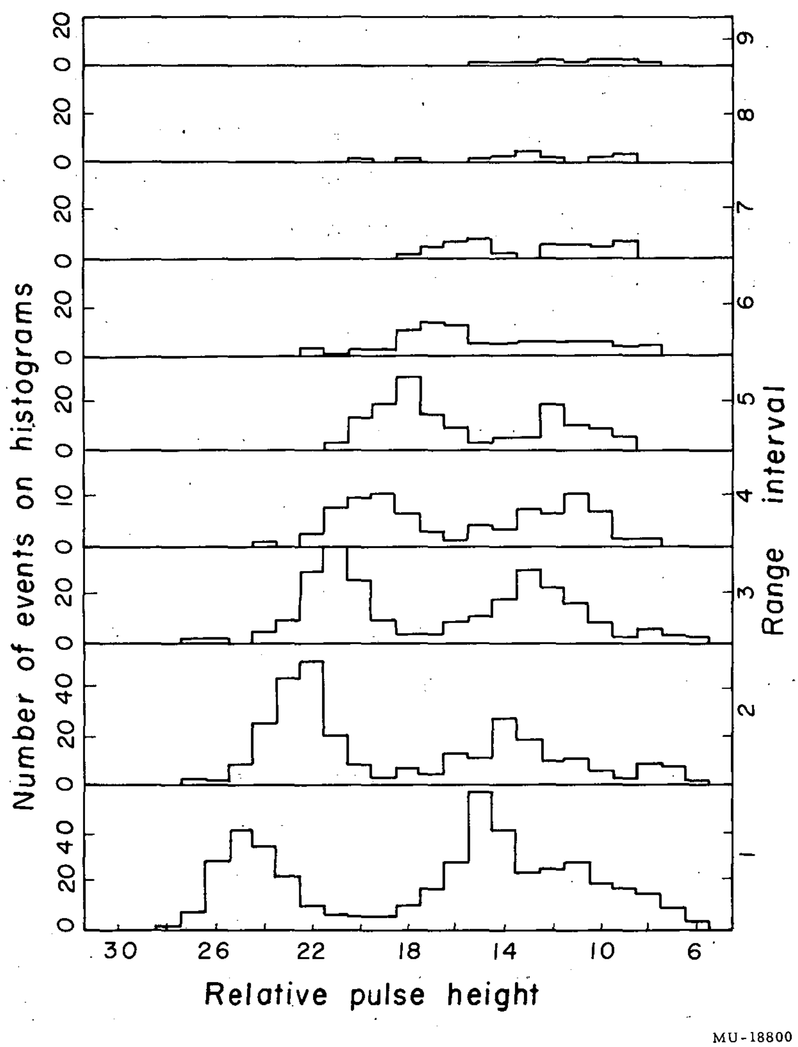

Fig. 7. Pulse-height spectra in the various range intervals obtained from charged particles produced at 60° by selected photons on carbon. These data include the accidental coincidences.

very-low-intensity beam of protons whose energy was set to correspond to each of the various range intervals in succession. From these spectra the protons in the higher energy intervals were determined.

All events in each range interval that had pulse heights in the dE/dx counter above a certain minimum were considered to be protons. This minimum pulse height was taken to be at that point between the proton and meson peaks on each histogram where the number of events reached a minimum. In the higher range intervals, where there were no separate peaks, this minimum pulse height was determined from the cyclotron run.

C. Corrections to the Proton Spectrum

1. Range Straggling

The most important correction was range straggling of the protons in the telescope due to nuclear collisions. It is virtually impossible to calculate this correction for a telescope such as was used in this experiment. This is because nuclear collisions often produce reaction products that traverse one or more additional range counters. Thus, for such a calculation, a knowledge of all the charged reaction products and their energy and angular spectra at all proton energies would be necessary. Because this information is not available it was decided to determine the correction from the previously mentioned calibration run at the 184-inch cyclotron.

In this run the external proton beam with energy reduced to about 300 Mev was allowed to strike a thick target. Protons of various energies corresponding to the range intervals of the telescope were then selected by a bending magnet as shown in Fig. 8. The results of a typical run are shown in Fig. 9. The coordinates have the same meaning as in Fig. 7. Each histogram represents the pulse-height spectrum of those events whose range interval is indicated on the abscissa. For this case the protons had an energy which should have allowed them to reach range interval No. 8.

Unfortunately there were many low-energy protons incident on the telescope in addition to those selected by the bending magnet. These protons undoubtedly resulted from scattering by the collimators

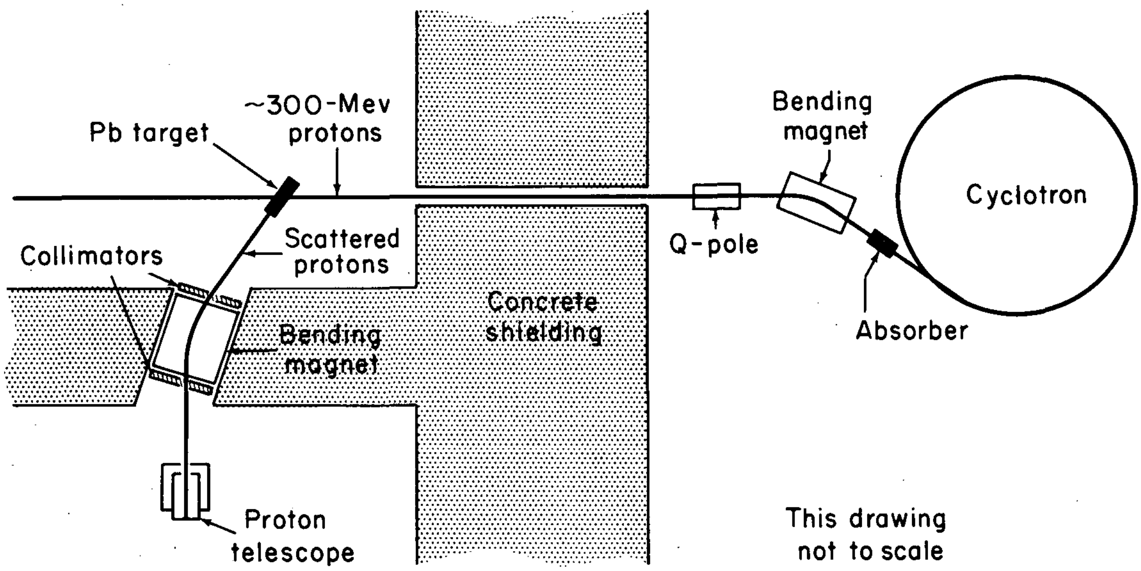

MU-18807

Fig. 8. Plan view of the experimental arrangement used in the cyclotron calibration run.

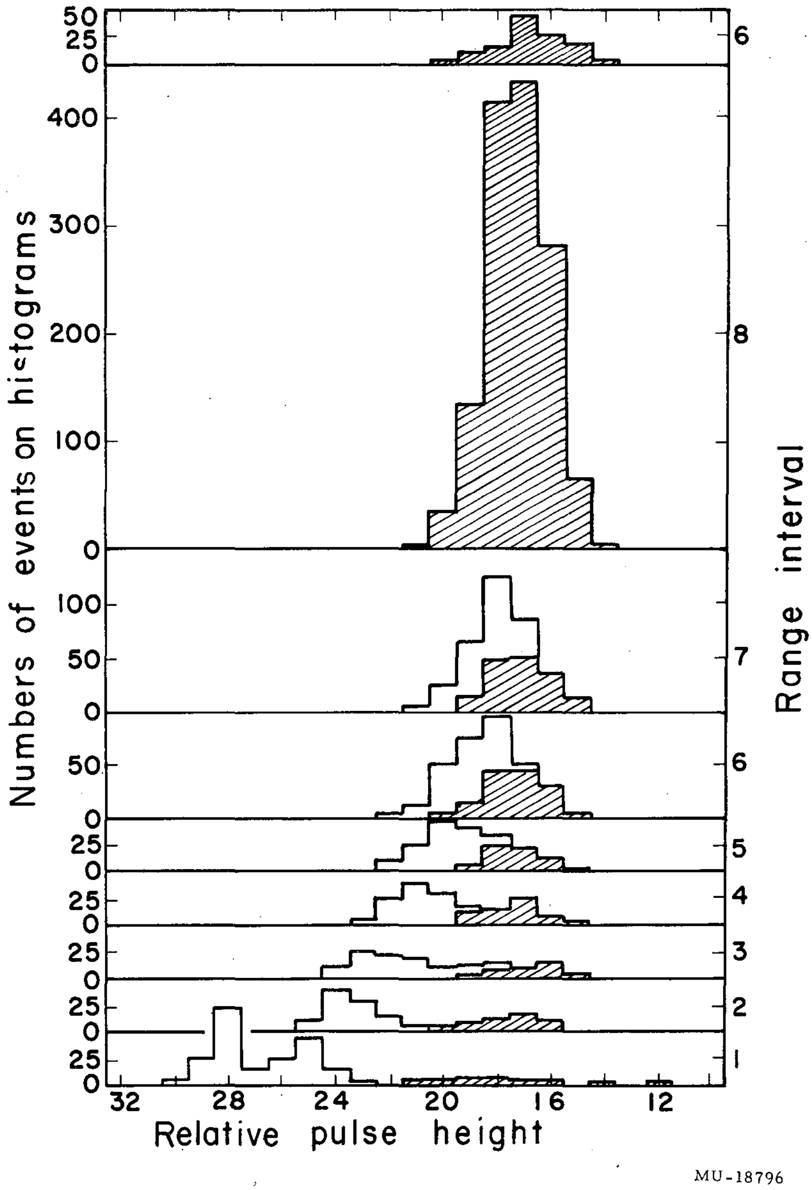

Fig. 9. Pulse-height spectra in the various range intervals obtained in that calibration run in which the incident protons had a proper range corresponding to range interval No. 8. The shaded areas represent protons that should have reached range interval No. 8. The unshaded areas represent the low-energy protons in the incident beam.

in the bending magnet. One thus sees two groups of pulse heights in the histograms of the lower range intervals. For example, on Fig. 9 in range interval No. 2 there is one peak in the pulse-height spectrum at a pulse height of 17, and another one at a pulse height of 24.

One group of protons had in each range interval a pulse-height spectrum that was the same as that in range interval No. 8. These are protons that would have reached range interval No. 8 if it had not been for some nuclear event. The other group, due to the low-energy protons, had a pulse-height spectrum in each range interval appropriate to its observed range. The pulse-height spectrum as a function of range shows a behaviour similar to that for the proton data in Fig. 7.

In order to facilitate separating the two groups of protons, two demands were made on the data. First, the low-energy protons were required to have a pulse-height spectrum in each range interval appropriate to protons of that same range. Second, all the remaining protons had to have a pulse-height spectrum identical to that of the incident protons which reached their proper ranges, excluding the low-energy protons. For example, in Fig. 9, we required that the protons in range interval No. 2 whose pulse heights grouped around 17, have a pulse-height spectrum of the same form and occur at the same position as those which stopped in range interval No. 8. The protons grouped around pulse height 24 were then required to have a pulse-height spectrum appropriate to protons whose proper range put them in range interval No. 2.

The shaded areas in Fig. 9 represent those protons which should have reached range interval No. 8 but did not because of a nuclear collision. The unshaded areas represent the low-energy protons incident on the proton telescope.

The results of Fig. 9 are plotted in Fig. 10. It shows the precent loss of protons from range interval No. 8 into each range interval indicated on the abscissa. There is considerably more scatter in the points than would be allowed by the statistical errors. This is undoubtedly due to the difficulty in separating the two groups of protons. In particular, the points corresponding to range intervals Nos. 6 and 7 appear to be too high. This cannot be accounted for by

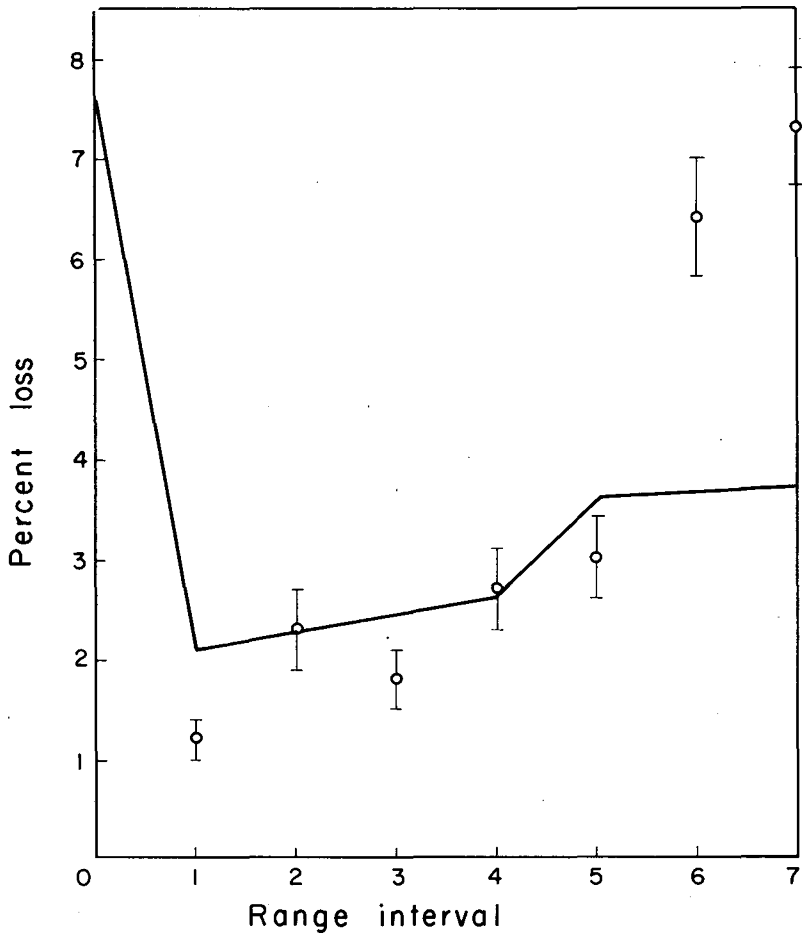

MU-18808

Fig. 10. Plot of the percent loss into range interval (given on the abscissa) of protons whose proper range corresponded to range interval No. 8. The curve represents the loss calculated on the assumption that the effective absorption cross section was 85% of the geometric cross section.

ionization range straggling. Furthermore, Dwight Dixon earlier measured the nuclear correction in this same telescope at lower energies by another method.[10] He did not observe this effect. We conclude that it was due to the difficulties associated with separating out the low-energy protons incident on the telescope.

To eliminate these systematic errors, the data were used to determine an effective nuclear mean free path for protons in matter at those energies at which the data appeared to be consistent. This mean free path was then assumed to be correct for all energies. It was also used to determine the absorption of protons before they reached the first range interval. In Fig. 10 this is called range interval 0. The mean free path determined in the above manner is the same as would be calculated from an absorption cross section that is 85% of the geometric cross section of the absorber nuclei. The range straggling predicted by this mean free path fits the data quite well in the lower range intervals, as can be seen from the curve in Fig. 10. It also fits reasonably well the data obtained when the protons incident on the telescope had lower energies. Elastic scattering did not contribute to loss of particles because the defining counter was considerably smaller than the range counters shown in Fig. 4.

The previously determined mean free path was used to determine a series of curves, such as the one in Fig. 9, representing the percentage loss into the various preceding channels of protons that should have reached each of the nine range intervals. From these curves the necessary corrections to the proton spectrum were made. An amount was added to each range interval to account for the loss of protons that should have reached this range interval, and an amount was subtracted to account for the protons that should have reached a higher range interval but which stopped in the one under consideration. The calculation was facilitated by starting with range interval No. 9 and working back to range interval No. 1, because no protons had a range that would carry them beyond range interval No. 9. This was because it was at the upper limit in energy allowed by conservation of energy. An experimental check was that the number of protons recorded by range counter 10 was zero. A correction was also made for those protons stopping before their proper range that showed a pulse height from the dE/dx counter which fell in the meson region of the pulse-height spectrum and therefore were not counted as protons.

Although it was not very precisely determined, the nuclear correction was small enough so that it had negligible effect on the conclusions drawn from this experiment. It did not alter any of the final data points by more than one probable error. The final corrections to the proton spectrum are shown in Table I.

Table I

Corrections due to range straggling

Range Interval	1	2	3	4	5	6	7	8	9
Correction (%)	1.4	5.9	7.4	8.8	12.6	15.8	18.5	20.9	33.0

2. Energy Loss in Target

Another correction was due to the energy loss of the protons within the target. The target was $2.21 g/cm^2$ thick. On the average, then, protons in the lowest energy interval lost about 8 Mev within the target and protons in the highest energy interval lost about 5 Mev. The experimental points were adjusted to compensate for this.

3. Nuclear Energy Loss

Some of the ejected protons suffered collisions with one or more of the other nucleons before leaving the target nucleus. The proton spectrum had to be corrected for energy loss due to this process. Just as in the range-straggling correction an amount had to be added to each range interval to account for those protons which should have reached this range interval but did not because of energy loss from collisions inside the target nucleus. Then also an amount had to be subtracted from each interval to account for those protons which should have reached a higher range interval but instead stopped in the one under consideration, again because they lost some of their energy before leaving the target nucleus. Consideration was given also to high-energy secondary protons resulting from collisions with the original protons and neutrons from the quasi deuteron.

Since this was a small correction (we shall verify this later), we used the approximate method of Weil and McDaniel.[4] For this calculation we assumed that the effective scattering cross sections inside the nucleus were 2/3 of the free cross sections.[12] The experimental values of σ_{np} and σ_{pp} were taken from Reference 13. From these cross sections an effective mean free path was calculated. This was used to calculate the probability of a proton's undergoing one or more collisions before leaving the nucleus. It was assumed that after a scattering event all energies were equally probable for the two particles from 20 Mev to E_p-10 Mev, where E_p is the initial energy of the particle. For single scattering a correction factor of 2 was applied, and for double scattering a correction factor of 4 was applied. Triple scattering was negligible. These correction factors resulted from considering the multiplicity of high-energy protons produced by these scattering events.

No correction was made for angular scattering in the target nuclei. It was assumed that the number of protons scattered into trajectories that would enter the telescope was equal to the number scattered out of such trajectories.

The corrections resulting from the above calculation are shown in Table II.

Table II

Corrections due to nuclear energy loss

Range Interval	1	2	3	4	5	6	7	8	9
Correction (%)	11	11	11	11	9	9	7	7	7

D. Calculation of the Cross Section

The cross section was calculated from the formula

$$N = \frac{d^2\sigma}{d\Omega dE_p} \; f \; t \; \Delta\Omega \, \Delta E_p \, , \tag{1}$$

where

N = number of events in a given energy interval,
f = number of selected photons,
$\Delta\Omega$ = solid angle,
ΔE_p = width of the given energy interval,
t = thickness of the target, in atoms/cm^2.

The solid angle of the proton telescope was just the solid angle subtended by the defining counter. It was 0.0276 steradian.

The carbon target has an effective thickness of 4.42 g/cm^2. Thus, t was 2.21×10^{23}/cm^2.

The flux of selected photons was determined from the measured efficiency of the electron counter and the total flux of photons, which was determined by means of a thick-walled ionization chamber of the Cornell type.

This chamber measures the total integrated energy of the photon beam.
We have

$$q = C \int_0^{E_m} E_\gamma \frac{dN_B}{dE_\gamma} \, dE_\gamma \, , \tag{2}$$

where
q = the collected charge on the ion chamber,
C = the calibration number of the chamber,
$\frac{dN_B}{dE_\gamma}$ = the bremsstrahlung differential spectrum of gamma rays traversing the chamber,

$E_m = 342$ Mev, the maximum gamma-ray energy.

We wish to determine the number of equivalent quanta Q, where

$$Q = \frac{1}{E_m} \int_0^{E_m} E_\gamma \frac{dN_B}{dE_\gamma} dE_\gamma . \tag{3}$$

From (2) and (3) we have

$$Q = \frac{q}{C} \frac{1}{E_m} . \tag{4}$$

For this chamber the calibration number is 3.79×10^{18} coulombs/Mev. It is believed to be accurate to within 5%.

If we write $$\frac{dN_B}{dE_\gamma} = \frac{N_o}{E_\gamma} , \tag{5}$$

then

$$Q = \frac{1}{E_m} \int_0^{E_m} \left(E_\gamma \frac{N_o}{E_\gamma} \right) dE_\gamma = N_o , \tag{6}$$

and we have

$$\frac{dN_B}{dE_\gamma} = \frac{Q}{E_\gamma} . \tag{7}$$

The number of selected quanta, N_{sq}, is thus

$$N_{sq} = \int_0^{E_m} e(E_\gamma) \frac{dN_B}{dE_\gamma} dE_\gamma = Q \int_0^{E_m} \frac{e(E_\gamma)}{E_\gamma} dE_\gamma, \tag{8}$$

where $e(E_\gamma)$ is the efficiency of the electron counter for observing an electron associated with a gamma ray of energy E_γ. Although the bremsstrahlung spectrum is not given precisely by $\frac{N_o}{E_\gamma}$, the error that this introduces is much smaller than the errors already present in the measured values of the electron-counter efficiency as a function of E_γ. The total number of selected photons that bombarded the target to give the data in Fig. 7 was 1.81×10^9.

V. RESULTS

The cross section is now readily calculated from Eq. (1). The results, after the correction of Tables I and II have been made and the accidentals subtracted off, are shown in Fig. 11. The errors indicated are the probable errors due to statistical uncertainty only. The data point corresponding to the ninth range interval is not shown (the experimental results were zero in this range interval).

In Fig. 12 is shown the differential cross section per equivalent quantum per nucleus for photoproton production from 342-Mev bremsstrahlung. This spectrum has been corrected for range straggling and energy loss from nuclear collisions, just as were the selected photon data. The corrections, of course, were slightly different because of the different spectrum obtained. No analysis of these data was made; they are shown for comparison only.

Two features of the results of Fig. 11 should be noted. One is the large high-energy tail in the proton spectrum up to the maximum energy allowed by conservation of energy. The other is the sharp maximum in the cross section at 119 Mev. The evidence for this rests primarily on the point at 105 Mev. If for some reason the efficiency of the first range counter in the proton telescope were lower than the others, the first point would be too low, showing a false peak at the next point. This does not seem likely, for two reasons. As previously indicated all the counters appeared to have 100% efficiency. Furthermore, the proton spectrum observed with the full bremsstrahlung spectrum of gamma rays showed no indication of a reduced efficiency in the first counter, as can be seen from Fig. 12.

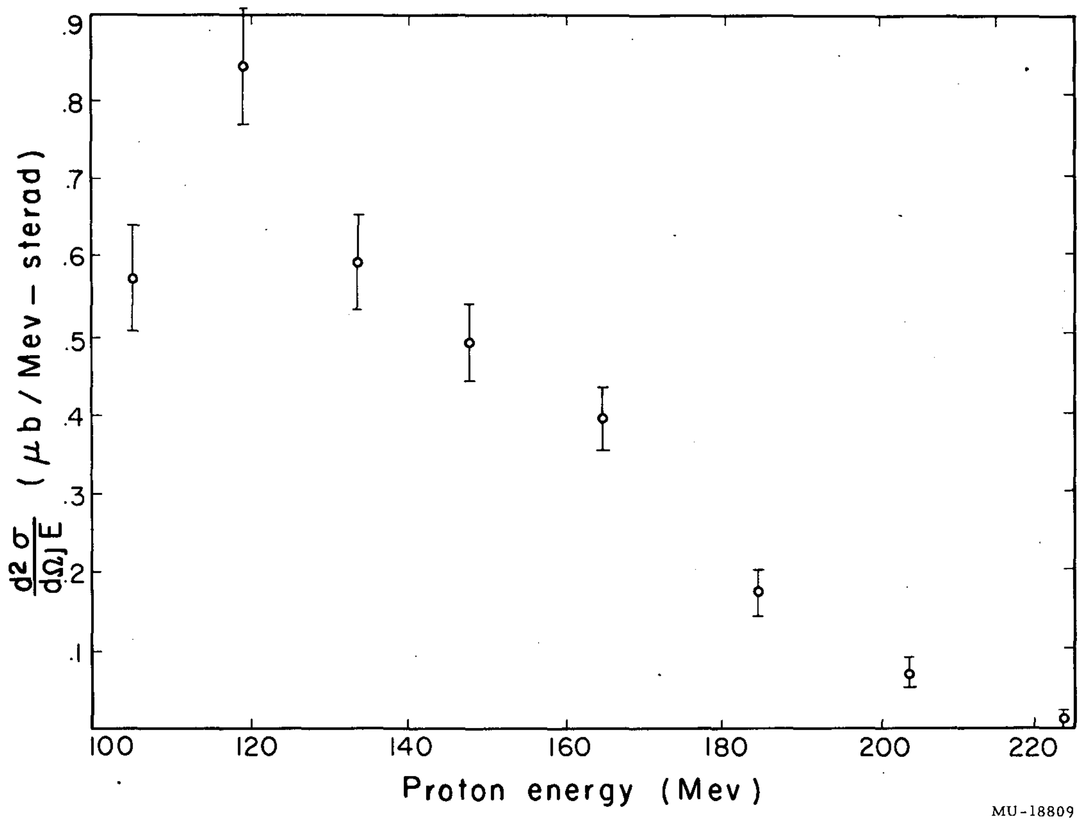

Fig. 11. Plot of the differential cross section per nucleus per selected photon for photoproton production from carbon at 60 deg by 245±15-Mev photons.

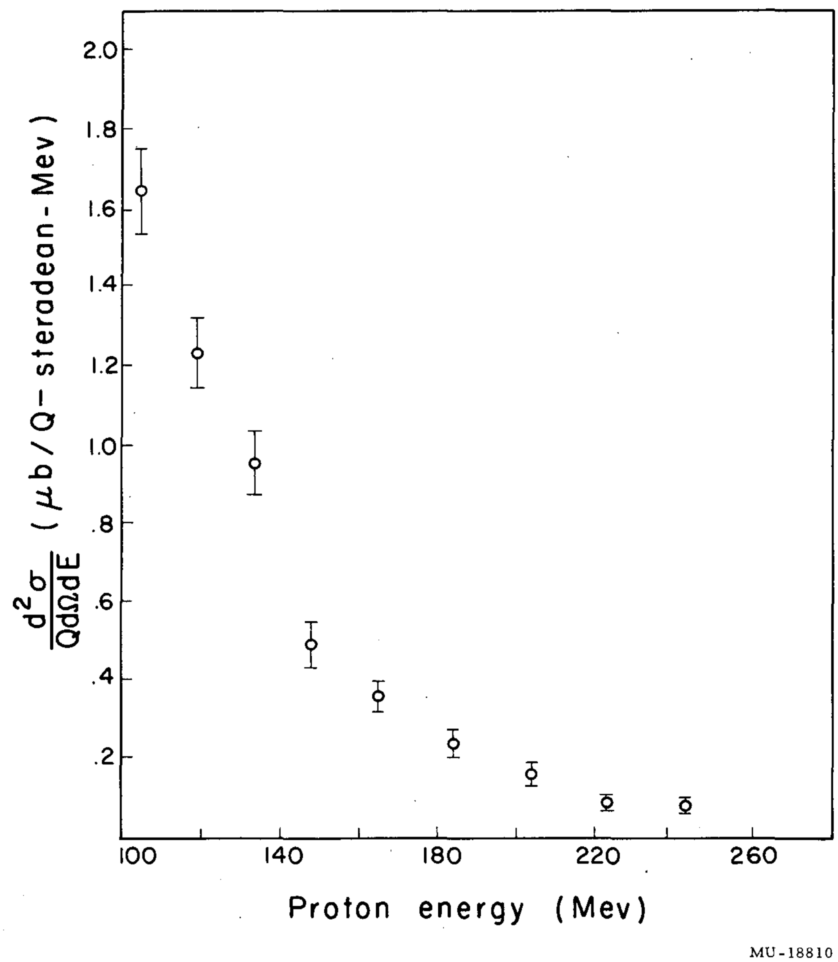

Fig. 12. Plot of the differential cross section per nucleus per equivalent quatum for photoprotons produced at 60 deg (lab) by bremsstrahlung on carbon.

VI. THEORY: CALCULATION OF THE CROSS SECTION

We now want to calculate the cross section implied by a given center-of-mass momentum distribution of neutron-proton pairs in the nucleus.

Using the quasi-deuteron model, we calculate the cross section from the kinematics of deuteron photodisintegration and then perform an appropriate average over the motions of all neutron-proton pairs in the nucleus. The resulting expression is

$$\sigma = \frac{1}{N_\gamma}\int \frac{dn_\gamma}{dE_\gamma}\,(1 - \beta_{zD})\,\frac{d^3N_D}{dP_D^3}\,\frac{d\sigma_D}{d\Omega_p}\,\delta(E_\gamma - B - E_p - E_n)$$
$$\times\, \delta^3(\vec{P}_\gamma + \vec{P}_D - \vec{P}_n - \vec{P}_p)\, dE_\gamma\, d\,P_D^3\, dP_n^3\, dE_p\, d\Omega_p \tag{9}$$

where

$$N_\gamma = \int \frac{dn_\gamma}{dE_\gamma}\, dE_\gamma\,, \tag{10}$$

σ = total cross section per photon per nucleus for the production of protons via the quasi-deuteron process,

$\frac{dn_\gamma}{dE_\gamma}$ = the energy spectrum of selected photons,

β_{zD} = the velocity of the quasi deuteron in units of c in the z direction (which is the direction assumed for the incoming photons),

$\frac{d^3N_D}{dP_D{}^3}$ = the momentum probability distribution of quasi deuterons inside the nucleus, normalized to total number of such pairs in the carbon nucleus,

$\frac{d\sigma_D}{d\Omega_p}$ = the differential cross section in the laboratory system for the photodisintegration of quasi deuterons moving inside the nucleus,

E_p, P_p, E_n, P_n = the kinetic energy and momentum of the final proton and neutron, respectively, after leaving the nucleus,

B = the sum of the binding energy of the neutron-proton pair in the nucleus plus the average excitation energy given to the nucleus remaining after the interaction.

The factor $(1 - \beta_{zD})$ corrects for the Doppler shifting of the photon flux.

The four delta functions in Eq. (9) ensure conservation of energy and momentum. It can be seen that the form of Eq. (9) evidently assumes that the energy and momentum of the final neutron and proton do not change as they leave the nuclear potential well. Refraction at the nuclear surface is thus ignored.

The finite aperture of the proton telescope is also ignored, since its angular width was only $\pm 8^\circ$.

Because the energy spectrum of selected photons was so narrow, it was assumed for the purpose of the calculation that all the photons had 245 Mev energy. The error that resulted from this approximation was small compared with the statistical errors in the data. Formally, in Eq. (9) we put

$$\frac{dn_\gamma}{dE_\gamma} = \delta(245 - E_\gamma). \tag{11}$$

From Eqs. (9) and (11) we can now write

$$\frac{d^2\sigma}{dE_p d\Omega_p} = \int (1 - \beta_{zD}) \frac{d^3N_D}{d P_D^3} \frac{d\sigma_D}{d\Omega_p} \delta(245 - B - E_p - E_n)$$
$$\delta^3\left(\frac{245}{c}\vec{k} + \vec{P}_D - \vec{P}_n - \vec{P}_p\right) d P_D^3 dP_n^3 , \tag{12}$$

where $\vec{k}$ is a unit vector in the z direction,

$$\frac{d^2\sigma}{dE_p\, d\Omega_p}$$ = the differential cross section per photon per nucleus for photoproton production.

The differential cross section (lab) for the photodisintegration of a quasi deuteron moving inside the nucleus was taken as

$$\frac{d\sigma_D}{d\Omega_p} = \left(\frac{r_I}{r_C}\right)^3 \left.\frac{d\sigma_D}{d\Omega_p}\right)_{free} , \qquad (13)$$

where r_I = the radius of interaction,

r_C = the radius of the carbon nucleus,

$\left.\frac{d\sigma_D}{d\Omega_p}\right)_{free}$ = the differential cross section (lab) for the photodisintegration of a free, moving deuteron. As is seen in Appendix A, it is a very complicated function of E_γ, $\vec{P}_D$, θ_p, and ϕ_p, where θ_p and ϕ_p are the laboratory-system angles of the proton.

The momentum-probability distribution of the quasi deuterons is normalized to the total number of neutron-proton pairs in the nucleus:

$$\int \frac{d^3N_D}{dP^3_D}\, dP^3_D = NZ, \qquad (13)$$

where N = the number of neutrons in the nucleus and Z = the number of protons in the nucleus.

The factor $\left(\frac{r_I}{r_C}\right)^3$ represents the probability that a neutron and a proton will be close enough to participate in the absorption of a photon. This quantity together with the normalization of $\frac{d^3N_D}{dP^3_D}$ gives the familiar NZ/A dependence of the cross section, where A = N + Z. The r_I was left as a free parameter in the calculation. We will see that, as expected, its value was of the order of the radius of the free deuteron for the momentum distributions that gave a reasonable fit to the data.

The $\left.\frac{d\sigma_D}{d\Omega_p}\right)_{free}$ was first determined in the rest system of the quasi deuteron. This corresponds to the laboratory system in the usual experiments on photodisintegration of deuterium. This quantity was approximated as

$$\left.\frac{d\sigma_D}{d\Omega'_p}\right)_{free} = 6.7+4.6 \cos\theta_{\gamma p}\ \mu b/\text{sterad.} \tag{14}$$

The ' indicates variables in the rest system of the deuteron. This expression is a good fit to the experimental data at $E_\gamma = 250$ Mev.[10] Furthermore, the cross section was assumed to be independent of energy. At these energies this is a good assumption. To transform to the laboratory system it is necessary to transform $\cos\theta_{\gamma P}$ and multiply the cross section by the appropriate Jacobian. These expressions are displayed in Appendix A.

By virtue of the threefold momentum δ function in Eq. (12) the integrations over P_n can be performed. One more integration can be carried out by using the energy δ function. This is chosen to be the integration over θ_D, the polar angle of the quasi deuteron. These integrations are shown in Appendix B. The result from Eq. (B11) in Appendix B, is

$$\frac{d^2\sigma}{dE_p d\Omega_p} = \frac{a}{\alpha}\int_{P_{min}}^{P_{max}} dP_D \int_0^{2\pi} d\phi_D (1-\beta_{\not{a}D}) P_D \frac{d^3N}{dP_D^3}\frac{d\sigma_D}{d\Omega_p}, \tag{15}$$

where $$a = 245 - B + E_p + Mc^2, \tag{16}$$

and $$\alpha = \sqrt{(245)^2 - 245\,P_p + P_p^2}\,. \tag{17}$$

The integration over ϕ_D from 0 to 2π and the integration over P_D from P_{min} to P_{max} were carried out numerically. The limits P_{min} and P_{max} are plotted in Fig. 13. The two limits become equal as shown at the upper limit of the proton energies allowed by conservation of energy.

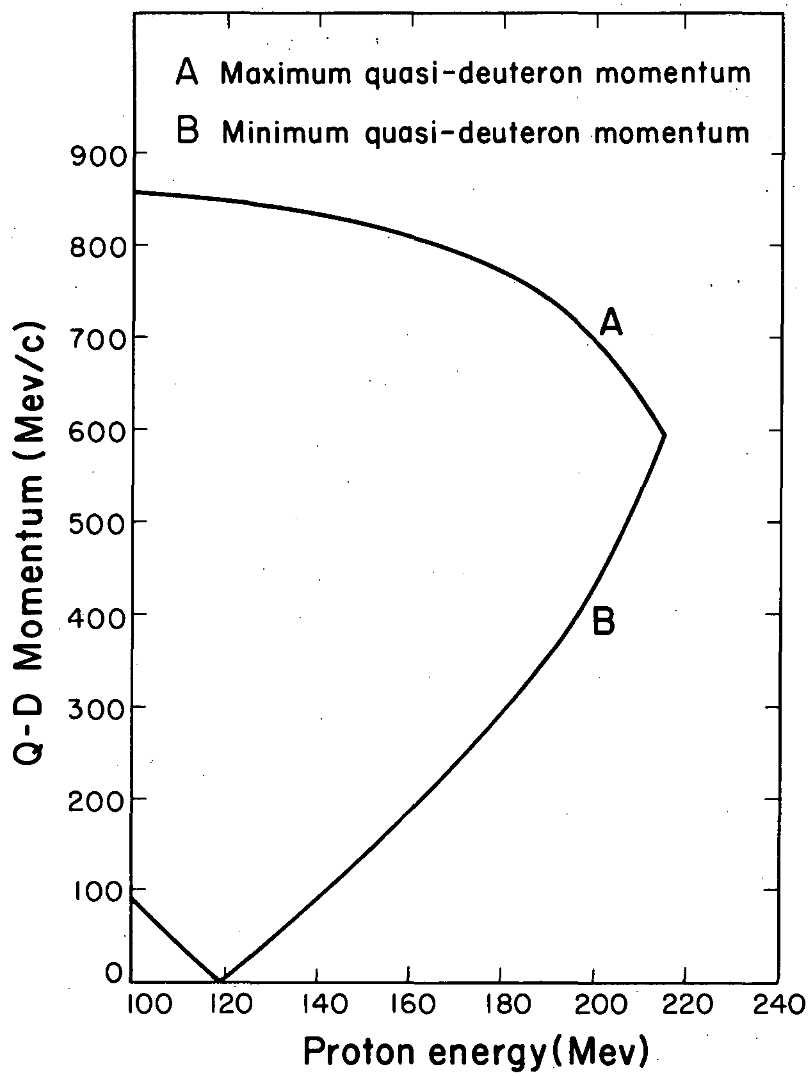

Fig. 13. Plot of the minimum and maximum quasi-momenta that can give rise to the proton energies, indicated on the abscissa, at 60° (lab). The two curves meet at the upper energy limit allowed by conservation of energy.

The integrand in the expression resulting from the integrations of the δ functions does not depend strongly on E_p, the proton energy. Therefore, the maximum in the differential cross section occurs approximately at that energy at which $P_{min} = 0$. This implies that the maximum in the differential cross section occurs at that proton energy which would be obtained by bombarding free deuterium with selected photons of the same energy. From the position of the maximum of the experimental cross section we can now determine B. We take this maximum as occurring at 119 Mev. This is the energy corresponding to range interval No. 2, which gave the highest experimental point. This gives

$$B = 35 \text{ Mev} \pm 5 \text{ Mev (estimated error)}$$

The estimated error is based on a crude estimate of the error in the position of the maximum of the differential cross section. A 5-Mev error in B implies a 5-Mev error in the position of the maximum. If we assume 7.5 Mev binding energy per nucleon in the carbon nucleus, the B = 35 Mev implies that the residual nucleus receives 20 Mev excitation energy on the average. The value of B also determines the upper limit of the proton energy allowed by conservation of energy. This energy is given simply by

$$E_p^{max} = E_\gamma - B + 7.5 \text{ Mev.} \qquad (18)$$

We add 7.5 Mev because at the upper limit the neutron need not leave the nucleus. For $E_\gamma = 245$ Mev then $E_p^{max} \cong 215$ Mev. From Fig. 11 we see that the proton spectrum does not appear to be quite zero at 215 Mev. This is undoubtedly because not all the gamma rays have exactly 245 Mev, as was assumed for the calculation. An appreciable number of gamma rays had energies as high as 260 Mev. Although this did not affect the calculation over most of the proton spectrum, it did cause some error near the upper limit of the spectrum.

It should be noted that the form of the energy δ function in Eq. (9) assumes that the quasi deuteron has constant binding energy in the nucleus. Because of this assumption the relative kinetic energy of the proton and neutron of the quasi deuteron never appear in the equations for the conservation of energy and momentum. This is because there are only two particles in the final state. It is assumed in the quasi-deuteron model that the incoming gamma ray transfers all its momentum and energy to a single neutron-proton pair. Any excitation energy received by the residual nucleus arises because the final neutron and proton undergo nuclear collisions before leaving the nucleus.

We can now verify our earlier qualitative statement concerning the smallness of the correction to the proton spectrum due to the energy loss from nuclear collisions of the final protons before leaving the target nucleus. We found that the average excitation energy given to the residual nucleus was 20 Mev. This means that in the photodisintegration of a quasi deuteron, the proton and neutron each lost an average of 10 Mev before leaving the nucleus. Since the proton energies observed in this experiment covered a range from 90 to 250 Mev, the protons lost an average of only 5 or 10% of their energy because of nuclear collisions.

VII. DISCUSSION AND CONCLUSIONS

The calculations were carried out for two quasi-deuteron momentum spectra. These are plotted in Fig. 14. These two spectra, labeled A and B in Fig. 14, have been given the same normalization. Except for this the normalization in the figure is arbitrary.

The proton energy spectra resulting from the previously outlined calculation when the momentum spectra in Fig. 14 are used, are shown in Fig. 15. The experimental data are shown also for comparison. The curves have been normalized to give the best least-squares fit to the data. This normalization determines r_I. For both momentum spectra the result is obtained that $r_I = 2.1$ fermis. Although this is of the order of the free deuteron radius, as expected, it is, nevertheless, considerably larger. However, this is not inconsistent with Levinger's model. He showed only that the quasi-deuteron wave function was proportional, but not equal, to the wave function of the free deuteron when the separation between the neutron and proton was small. The constant of proportionality depends on assumptions concerning the wave function for large separation of the neutron and proton.

The momentum-probability distribution designated as "A" was taken from the experiment of Wattenberg et al.[9] In that experiment the angular correlation between conjugate neutrons and protons from carbon was measured. A Gaussian function with a 1/e value of about 20 Mev gave a reasonable fit to their data. This is the momentum distribution which we call "A". The analysis by which they arrived at this momentum distribution was somewhat crude. It ignored conservation of energy and the fact that the incident gamma rays had a bremsstrahlung spectrum of energies. Our analysis, by contrast, was reasonably precise. As can be seen from Fig. 15, distribution "A" gives a fair fit to the data except in the region around 120 Mev. It does not give the sharp maximum exhibited by the experimental data.

The momentum distribution designated as "B" in Fig. 14 was constructed in an attempt to obtain a better fit to the data in the region around 120 Mev. It is clear from the form of Eq. (15), and from Fig. 13, that the only way to enhance this region without distorting the proton

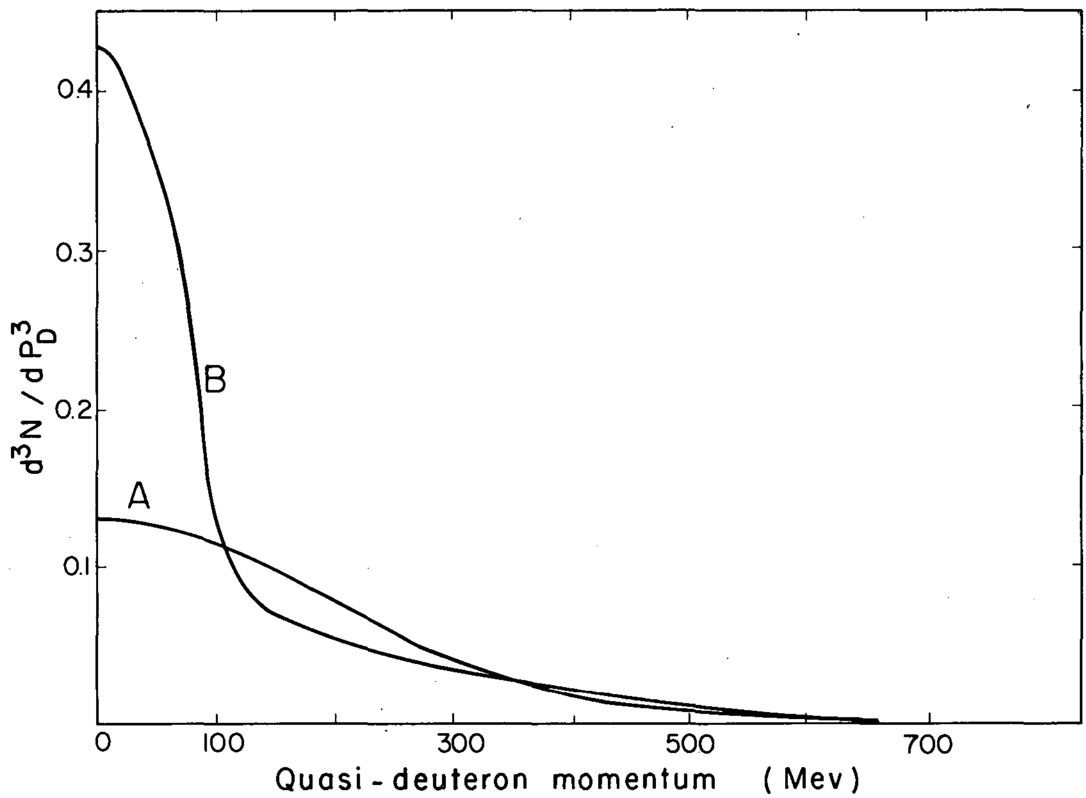

MU-18812

Fig. 14. Quasi-deuteron momentum spectra used in the calculations. The two curves have the same normalization. Except for this the normalization in the figure is arbitrary.

Curve A: $\dfrac{d^3N}{d\,P_D{}^3} = 0.13\ \exp\,(-P_D{}^2/4ME_1)$, $E_1 = 20$ Mev.

Curve B: $\dfrac{d^3N}{d\,P_D{}^3} = 0.36\ \exp\,(-P_D{}^2/4\ ME_2) + 0.07\ \exp\left(-\dfrac{P_D{}^2}{4ME_3}\right)$,

$E_2 = 1.6$ Mev, $E_3 = 30$ Mev.

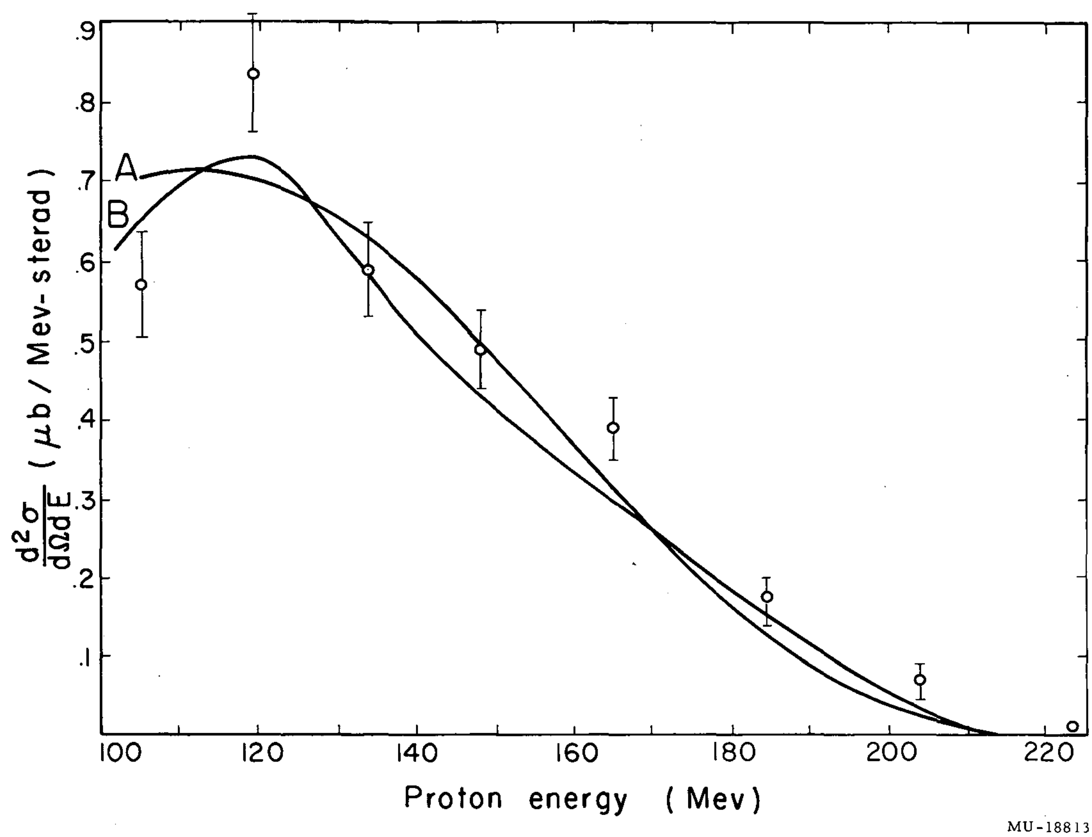

Fig. 15. Comparison between the experimental data and the results of the calculations using the momentum spectra shown in Figure 14.

energy spectrum at the higher energies is to give increased weight to the momentum spectrum in the region of low momenta. This is because these low momenta are included within the limits of integration only in the region near the maximum of the cross section.

Momentum distribution B is given by the sum of two gaussians, functions one with a 1/e value of 1.6 Mev and the other with a 1/e value of 30 Mev. From Fig. 15 we see that this momentum spectrum does give a fairly sharp maximum at about the right energy. To obtain it, however, the low momenta had to be enhanced by a very large amount, as is apparent from Fig. 14. This is because the available phase space for low momenta is much smaller than for high momenta. The least-squares error for momentum distribution "B" was about 20% less than that for "A".

By further enhancement of the low momenta, the fit to the data around 120 Mev could probably be improved. However, in view of the magnitude of the statistical errors present on the experimental points, it did not seem worth while further to refine the momentum spectrum. The necessary alteration that must be made is clear from the above discussion. This momentum distribution is already unusual enough to demand considerable discussion.

Two observations are pertinent. First, a neutron-proton pair is a boson. This means that there is no Pauli principle to prohibit putting many quasi deuterons in the same state. Thus it is possible for them to pile up in the low momentum states. This would be indicated by the momentum probability distribution "B". The individual neutrons and protons could, of course, still retain their own characteristic momentum distributions. These particles would, however, not be randomly distributed, but would instead be correlated through the momentum distribution of the centers of mass of pairs of nucleons.

Second, there is considerable evidence that the large momenta observed for single nucleons inside the nucleus are due to two-body correlations.[14] If this is true, then the momentum-probability distribution of pairs of nucleons should be narrower than would be predicted from a random distribution of nucleons in the nucleus. The work of Cladis, Hess, and Moyer indicates that the protons in the carbon nucleus can be fitted to a Gaussian momentum distribution with a 1/e value of 16±3 Mev.[15]

Random mixing of pairs of nucleons would give again a Gaussian distribution with a 1/e value of 16 Mev. Distribution "A" (taken from Wattenburg et al.) implies, then, random mixing of pairs of nucleons. While it is not clear what form the "narrowing" of the probability distribution of pairs of nucleons would take if there really were large two-body correlations, it is clear that momentum distribution "B" differs from "A" in the right direction. It should be emphasized that only the qualitative differences between momentum spectra "A" and "B" are considered significant.

The evidence for the large enhancement of the low momenta of the quasi deuterons rests entirely on the sharp peak in the energy distribution of the ejected protons near 120 Mev, as indicated by this experiment. This is the first experiment to show such a peak. It is obvious why experiments with bremsstrahlung would not show such a peak, since all gamma-ray energies are present down to zero energy. Weil and McDaniel did not see a peak in the energy distribution of protons because in their experiment (a) the energy spectrum of selected photons was quite broad (190±30 Mev compared with our 245±15Mev), (b) the angular aperture of their proton telescope was large (±15° compared with our ±8°), and (c) protons were observed in a lower energy region (40 Mev to 200 Mev compared with our 90 Mev to 250 Mev), which meant that the nuclear-scattering correction was more severe.

It is clear that the work of this experiment ought to be continued in order to improve the accuracy of the data, to explore more of the region below 120 Mev proton energy, and to verify the apparent sharp maximum in the differential cross section. (To facilitate this it will be important to construct an electron counter with near 100% efficiency for counting electrons even under the unfavorable conditions required. The statistical errors present in the data of this experiment are so large that little more than qualitative statements can be made about the momentum spectrum of quasi deuterons in the nucleus. We feel, however, that selected photons have proven themselves useful for probing nuclear internal momenta. In particular, an accurate determination of the quasi-deuteron momentum spectrum would give considerable information concerning the supposed two-body correlations in the nucleus. It would not be possible to attain by the subtraction technique the energy selection of gamma rays obtained in this experiment.

Another reason to obtain more accurate data is to determine better the differential cross section in the region around 165 Mev proton energy. There is some slight indication of a "shoulder" in the cross section in this energy region. This is about 2/3 of the gamma-ray energy. Protons of this energy would result from a three-body interaction in which two of the particles were bound, or at least highly correlated, in the final state. This interpretation is not stressed, because the statistical errors are large enough so that this effect could be a statistical fluctuation. More accurate data would resolve this ambiguity.

Finally, it is possible from the results of this experiment to set a lower limit on the maximum quasi-deuteron energies present in the carbon nucleus. The highest proton energies present can be estimated from Fig. 11. We estimate them as 210 Mev. P_{min}, corresponding to this proton energy, in Eq. (15), can be obtained from Fig. 13. It is about 530 Mev/c. This means that there must be quasi deuterons with momenta greater than 530 Mev/c or about 80 Mev kinetic energy. This requires then that there must be individual nucleons with energy greater than 40 Mev in the carbon nucleus. It would be possible to get this same kind of information about even higher quasi-deuteron momenta by observing protons at larger angles. Of course the cross section falls rapidly as the proton angle is increased.

ACKNOWLEDGMENTS

I would like first to express my gratitude to Professor Moyer for his timely advice throughout the course of the experiment. Also I would like to thank Gilbert Mead for his generous assistance in the final stages. Finally I would like to thank Rudin Johnson and the synchrotron crew for their enthusiastic cooperation in carrying out the many unusual requests made in connection with this experiment.

This work was done under the auspices of the U. S. Atomic Energy Commission.

APPENDIX A

We set $M_n = 1$, $c = 1$, and write

$$p_x = p_D \sin\theta_D \cos\phi_D, \tag{A1}$$

$$p_y = p_D \sin\theta_D \sin\phi_D, \tag{A2}$$

$$p_z = p_D \cos\theta_D, \tag{A3}$$

where θ_D, ϕ_D are the quasi-deuteron angles in the laboratory system. Then at laboratory-system angles $\theta_p = 60^\circ$, $\phi_p = 90^\circ$ we have

$$\cos\theta_{\gamma p} = \frac{1/2\left(1 - 1/2\, p_z - \frac{\sqrt{3}}{2}\, p_y \frac{p_z}{\beta_p} + \frac{1}{2}\frac{p_D^2}{\beta_p^2}\right)}{\left[1 - p_z + 1/4\, p_D^2\right]^{1/2}\left[1 - \frac{1}{2\beta_p}\left(\sqrt{3}p_y + p_z\right) + 1/4\,\frac{p_D^2}{\beta_p^2}\right]^{1/2}} \tag{A4}$$

where β_p = velocity of the proton in units of c.
The appropriate Jacobian is

$$J = J\left(\frac{\cos\theta_{\gamma p},\ \phi_{\gamma p}}{\cos\theta_p,\ \phi_p}\right) = \begin{vmatrix} \dfrac{\partial\cos\theta_{\gamma p}}{\partial\cos\theta_p} & \dfrac{\partial\phi_{\gamma p}}{\partial\cos\theta_p} \\[2ex] \dfrac{\partial\cos\theta_{\gamma p}}{\partial\phi_p} & \dfrac{\partial\phi_{\gamma p}}{\partial\phi_p} \end{vmatrix}, \tag{A5}$$

$\theta_{\gamma p}$, $\phi_{\gamma p}$ = angles between the direction of the gamma ray and the proton in the rest system of the quasi deuteron,

θ_p, ϕ_p = angles of the protons in the laboratory system.

We have, finally,

$$J = \frac{\frac{1}{8}\left[1-\frac{p_z}{\beta_p}\right]\left[\left(\frac{p_y}{\beta_p}-\sqrt{3}p_{\cancel{z}}\right)\left(\frac{p_y}{\beta_p}-\sqrt{3}\right)+\frac{p_x^2}{\beta_p^2}\right]-\frac{\sqrt{3}}{2}\left[1-\frac{1}{2\beta_p}\left(\sqrt{3}\,p_y+p_{\cancel{z}}\right)+\frac{1}{4}\frac{p_D^2}{\beta_p^2}\right]\left[\frac{p_y}{\beta_p}-\sqrt{3}\right]}{\left[1-\frac{1}{2\beta_p}\left(\sqrt{3}\,p_y+p_{\cancel{z}}\right)+\frac{1}{4}\frac{p_D^2}{\beta_p^2}\right]^{3/2}\left[\frac{3}{2}-\sqrt{3}\frac{p_y}{\beta_p}+\frac{1}{2\beta_p^2}\left(p_x^{\,2}+p_y^{\,2}\right)\right]} \qquad \text{(A6)}$$

In order that the integral in Eq. (B3) be $\neq 0$, we must have

$$\sqrt{b-2a\,P_D+P_D^2} \leqslant a \leqslant \sqrt{b+2a\,P_D+P_D^2} \;; \qquad \text{(B12)}$$

P_{min} and P_{max} are deduced from Eq. (B12). The results are

$$P_{min} = \left|\, a - \sqrt{a^2-\mu}\,\right| \qquad \text{(B13)}$$

$$P_{max} = a + \sqrt{a^2-\mu} \qquad \text{(B14)}$$

where $\mu = 4T_p + 2(245)(-1/2\,P_D + E_p - M) + 2B(245 - E_p + M)$. (B15)

The P_{min} and P_{max} in Eq. (B13) for B = 35 Mev are plotted in Fig. 13. The expressions in Appendix A are now put into the expression for $\frac{d\sigma}{d\Omega_p}$ in Eq. (B11). The integrations over P_D and ϕ_D are then performed numerically by using the momentum spectra of Fig. 14. The results are shown in Fig. 15.

APPENDIX B

Equation (12) in the text can be integrated immediately to give

$$\frac{d^2\sigma}{dE_p d\Omega_p} = \int (1-\beta_{zD}) \frac{d^3N}{dP_D^3} \frac{d\sigma_D}{d\Omega_p} \delta(245 - B - E_p - \sqrt{P_n^2+M^2} + M) \, d\, P_D^3 , \tag{B1}$$

$$\text{where } P_n^2 = P_\gamma^2 + P_D^2 + P_p^2 + 2(\vec{P}_\gamma \cdot \vec{P}_D - \vec{P}_\gamma \cdot \vec{P}_p - \vec{P}_D \cdot \vec{P}_p) , \tag{B2}$$

and where we have put $c = 1$.

Remembering that $\vec{P}_\gamma$ defines the direction of the polar axis, we can write

$$\frac{d^2\sigma}{dE_p d\Omega_p} = \int (1-\beta_{zD}) \frac{d^3N}{dP_D^3} \frac{d\sigma_D}{d\Omega_D} \delta(a - \sqrt{b+2cP_D+P_D^2}) \, P_D^2 \, d\, P_D \, d \cos\theta_D d\phi_D , \tag{B3}$$

where $$a = 245 - B + E_p + M, \tag{B4}$$

$$b = P_\gamma^2 + P_p^2 + M^2 - 2\vec{P}_\gamma \cdot \vec{P}_p \cos\theta_p , \tag{B5}$$

$$c = (1/P_D \left[245 \cos\theta_D - P_p \cos\theta_D \cos\theta_p - P_p \sin\theta_p \sin\theta_D \cos(\phi_D - \phi_p) \right] . \tag{B6}$$

We now perform a rotation of the coordinate system of the quasi-deuteron system:

$$\begin{aligned} x &= x', \\ y &= y'\cos\psi - z'\sin\psi, \\ z &= z'\cos\psi + y'\sin\psi, \end{aligned} \tag{B7}$$

where $$\cos\psi = \frac{a}{\sqrt{a^2+b^2}} . \tag{B8}$$

We then have $$c = \alpha \cos\theta'_D , \tag{B9}$$

where $\alpha = \sqrt{(245)^2 - 245P_p + P_p^2}$, (B10)

and where we have assumed $\phi_p = 90^\circ$, as in Appendix **A**. Putting Eq. (B9) into (B3) and integrating over $\cos\theta'_D$, we have

$$\frac{d^2\sigma}{dE_p d\Omega_p} = \int (1-\beta_{\pi D}) \frac{d^3N}{dP_D^3} \frac{d\sigma_D}{d\Omega_P} \frac{a}{\alpha P_D} P_D^2 \, dP_D \, d\phi_D$$

$$= \frac{a}{\alpha} \int_{P_{min}}^{P_{max}} dP_D \int_0^{2\pi} d\phi_D \, (1-\beta_{\pi D}) P_D \frac{d^3N}{\alpha P_D^3} \frac{d\sigma_D}{d\Omega_P} .$$

(B11)

REFERENCES

1. J. C. Keck, Phys. Rev. 85, 410 (1952).
2. J. W. Rosengren and J. M. Dudley, Phys. Rev. 89, 603 (1953).
3. Feld, Godbole, Odian, Scherb, Stein and Wattenberg, Phys. Rev. 94, 1000 (1954).
4. J. W. Weil and B. D. McDaniel, Phys. Rev. 92, 391 (1953).
5. J. S. Levinger, Phys. Rev. 84, 43 (1951).
6. M. Q. Barton and J. H. Smith, Phys. Rev. 95, 573 (1954).
7. Myers, Odian, Stein, and Wattenberg, Phys. Rev. 95, 576 (1954).
8. M. Q. Barton and J. H. Smith, Phys. Rev. 110, 1143 (1958).
9. Wattenberg, Odian, Stein, Wilson, and Weinstein, Phys. Rev. 104, 1710 (1956).
10. Dwight R. Dixon, Photodisintegration of Deuterons at High Energies, UCRL-2956, Mar. 1955.
11. William A. Wenzel, Millimicrosecond Coincidence Circuit for High-Speed Counting, UCRL-8000, Oct. 1957.
12. Fernbach, Serber, and Taylor, Phys. Rev. 75, 1352 (1949).
13. Wilmot N. Hess, A Summary of High-Energy Nucleon-Nucleon Cross-Section Data, UCRL-4639, Jan. 1956.
14. Brueckner, Eden, and Francis, Phys. Rev. 98, 1445 (1955).
15. Cladis, Hess, and Moyer, Phys. Rev. 87, 425 (1952).